The role of wall deposition and re-entrainment in swirl spray dryers

Francia Garcia, Victor; Martín, Luis; Bayly, Andrew E.; Simmons, Mark J. H.

DOI:
10.1002/aic.14767

Document Version
Early version, also known as pre-print

Citation for published version (Harvard):
Francia Garcia, V, Martín, L, Bayly, AE & Simmons, MJH 2015, 'The role of wall deposition and re-entrainment in swirl spray dryers', *AIChE Journal*, vol. 61, no. 6, pp. 1804–1821. https://doi.org/10.1002/aic.14767

EXPERIMENTAL EVIDENCE OF THE ROLE OF WALL DEPOSITION AND RE-ENTRAINMENT IN SPRAY DRYERS USING TURBULENT SWIRLING FLOWS

Victor Francia[i,ii,*], Luis Martin[ii],Andrew E. Bayly[ii,] , Mark J.H.Simmons[i]

[i]*School of Chemical Engineering, University of Birmingham, Birmingham, United Kingdom.*
[ii]*Procter & Gamble R &D, Newcastle Innovation Centre, Newcastle upon Tyne, United Kingdom.*

* corresponding author, v.francia.chemeng@gmail.com

Keywords: deposition, re-entrainment, fouling, re-suspension, spray drying.

Abstract

This paper investigates the dynamics of fouling during the manufacture of detergents in a swirl counter current spray dryer using a tracer. Deposits grow as multiple layers, break up and cause re-suspension of material. Identification of the aggregates originated at the wall shows, remarkably, that $> 20\ \%$ by mass of the product is re-entrained from the deposits and experiences residence times ten to a hundred times higher than expected from the air flow patterns. The interaction with the wall explains the formation of the largest particles, which are aggregates of droplets and deposits.

This work introduces a residence time approach to characterise fouling in powder manufacturing. In the context studied, the data reveals the wall dynamics is critical to define product attributes and must be addressed numerically. A description of the micro-mechanics of the wall-borne processes has been proposed including dry and wet mechanisms of erosion caused by particle impacts.

1. Introduction.

Fouling remains a fundamental issue in many industries and involves the mechanisms by which discrete particles, clusters, floccules or colloidal structures deposit at the walls of contained units. It is often a dynamic process where the deposits are re-suspended by the action of aerodynamic forces, gravity or impacting particles. Colloidal, biological or particulate deposits are formidable technical challenges in applications across the petrochemical industry, aerosols and engines, membrane processes, medical applications and within many operations in the particle technology industry, from packaging to granulation or spray drying.

The underpinning physics of fouling is intimately related to the particle turbulence interaction (Papavergos and Hedley 1984). As particle relaxation time increases deposition and re-entrainment become governed by inertial effects and less influenced by turbulent flow. Several studies thus focus on the interactions between small particles and near-wall boundary layers, for example Ziskind *et al.* (1995) or Soldati and Marchioli (2009) describe how coherent turbulent structures near the wall are responsible for unbalanced rates of deposition and ejection events. These systems usually deal with single particles and mono-layers, disregarding particle-particle forces and focusing on describing the interaction between the particles and the surface. Henry *et al.* (2012) reviews in detail the work in colloidal particulate fouling, where a number of authors work in a multi-layer description including the interaction force between the wall-borne clusters. A different approach to re-suspension has also been proposed by Reeks *et al.* (1988) and Reeks and Hall (2001) based on the description of a potential, or energy well, this was later extended to a multi-layer kinetic description by Zhang *et al*. (2013). Other important effects include the impact of swirling flows (Zonta *et al.* 2013), wall roughness (Guingo and Minier 2008) or the formation of aggregates near the wall (Marshall 2007).

The study of lower ranges of inertia focuses on short range adhesive and cohesive forces such as Van der Waals or electrostatics, and often associates the cause of re-entrainment to an aerodynamic origin. However, gravity driven mechanisms such as the detachment of large sections, or shedding, are also studied in fields such as combustion. Ash deposition, aging and shedding are recognized phenomena in the comprehensive descriptions given by Wang and Harb (1997) or Zbogar *et al.* (2009) and in the experiments from Bashir *et al.* (2012).

The effect of particle impacts at higher particle inertia can lead to re-suspension, which has received little attention, not the least due to the difficulties in describing their microstructure (Kota and Langrish 2006). Deposits in industry comprise of a wide range of different materials. This involves many types of different interactions, cohesive forces and aging processes. Reproducing their structure experimentally is extremely challenging, which explains the lack of data and the use of semi-empirical models for design purposes (e.g. Epstein 1983).

Regimes covering high particle inertias occur in the spray drying of products such as milk, instant coffee, pharmaceutical powders, ceramics or detergents. Here, particles and droplets with a wide range of size, momentum and composition coexist in the unit. The study of deposition and re-entrainment has mostly focused on co-current dryers and has been associated with three main issues: 1- product degradation and safety and quality concerns, 2- a detriment in the yield and the process efficiency and 3- costs associated to maintenance (Ozmen and Langrish 2003). The research undertaken in the context of the food industry reports ample evidence in this regard (e.g. Kota and Langrish 2006). It provides the most relevant efforts in optimizing the yield (e.g. Langrish and Zbiciński 1994; Hanus and Langrish 2007a; Kota and Langrish 2007), for which the role of re-suspension is emphasized (Hanus and Langrish 2007b) and particle-wall contact models are being developed (Woo *et al.* 2010). Counter-current spray dryers operate differently: they benefit from a strong turbulent swirling flow to increase particle residence time and obtain better energy efficiencies (Huntington 2004). On the one hand, the counter flow causes an increase in particle concentrations, promoting particle-particle contacts and agglomeration (Palzer 2011) whilst on the other, the swirling motion generates a preferential concentration of particles near the wall, where certain size fractions tend to stagnation. This causes multiple wall impacts and much higher deposition rates. However, very few works pay attention to the wall processes in these units. In a detergent context they have been largely linked to operational issues (Huntington 2004) rather than to any significant effect to the process. Only recently the work of Hassall (2011) acknowledged the generation and breakage of particulate multi-layers at the walls, providing visualization of the near wall region in a restricted area. A detailed study of these processes remains a challenging task because it deals with complex contact mechanics when deformable droplets or semi-dried particles impact a fixed substrate, comprised itself of clusters.

In co-current dryers the yield decreases due to material accumulating at the wall (Ozmen and Langrish 2003; Hanus and Langrish 2007b). However, it must be noted that swirl counter-current towers operate for long periods of time without the need for cleaning. It follows that deposition is either suppressed, or balanced by the re-entrainment of material. Perhaps a more revealing question would be the time scale over which this equilibrium is reached. In general, the frequency of re-entrainment events in any given structure is owed to a balance between disruptive stresses and cohesive forces. If the stresses are low, large clusters are re-entrained, few events occur and their time scale is high, potentially larger than the process time scale. In this case, re-entrainment is observed as intermittent events and produces particles clearly identifiable by a large size and a different structure from the rest of particles in the flow. This is for instance the case of shedding of ash deposits in burners (Zbogar *et al.* 2009). On the contrary, if disruptive stresses are much higher than any bonds between particles or particles to the wall the re-entrainment events are much more frequent and particles spend no significant time in contact to the wall. The work presented in later sections confirms that the deposits seen in a swirl counter current detergent spray dryers are an intermediate scenario. Disruptive stresses are comparable to the structural forces binding the clusters together and re-entrainment events become more frequent than in a shedding process. The time scale of the contact with the wall now approaches that of the process and the sizes of the re-suspended clusters becomes comparable to the mean product size (Hasall 2011). For that reason, the aggregates originated at the wall simply blend in with the rest of particles in the product, which explains why they have never been characterised.

Current numerical models of spray dryers assume that the wall has a minor contribution to the overall process and

ignore any significant impact in particle residence time or growth, which have not yet been studied in detail. This is the purpose of this work. The following sections focus in the study of an industrial scale detergent counter-current spray drying tower. They outline a tracer experiment that has permitted quantification of the re-entrainment, and analysis of its impact in the residence time of the solids and the size of the final product. The data underscore the errors associated with the omission of the wall processes in numerical models, failing to account major effects in the particle drying and growth of large part of the product, including the majority of granules of a size $> 850\ \mu m$.

2. Experimental methodology.

2.1. Unit design and operation.

A spray drying tower, property of Procter & Gamble Co was used in the experiments. The design and operation are depicted in Figures 1. The hot air is introduced at the bottom of the tower through a series of symmetrical air inlets [5], which impart downwards and tangential components to the air velocity. Their action causes an air vortex to rise into the cylindrical section and the kinetic energy contained in the flow, in particular within the tangential motion, decreases due to the action of the wall shear stress, which leads to recirculation and instabilities (Francia *et al.* 2014a, 2014b). Upon reaching the top end of the cylinder, the flow converges into the tubular guard or vortex finder, and exits towards cyclones [23] where the elutriated fines [26] are separated from the exhaust air [25].

A standard detergent formulation serves for the preparation of the slurry, which is comprised of aqueous, organic and solid phases. It is generated in a batch mixer, known as the crutcher [7] by the addition among others of polymer/s, surfactant/s and inorganic salts, for an overall content in solids between $30 - 60\%$ in mass. A larger mixer, or homogenizer, known a drop tank [8] serves as the buffer for continuous operation. The slurry is then pumped at a low pressure into a hammer mill [13] to break agglomerates and avoid damage and blockages downstream. It is then brought to high pressure and conducted into the tower [15]. Atomization is performed from a single swirl pressure nozzle that provides a hollow cone pattern (Huntington 2004). It is located at the level $5.9\ D$ [17], at the centreline and aligned downwards. Inspection areas at the walls are shown in Figure 2 and Table 1 summarizes the main operation conditions.

Three modifications were made to conduct the tracer experiments, see Figure 1: 1- an injection system for an aqueous solution of dye is installed at the low pressure line [11,12, before the hammer mill; set to provide $100\ ppm$ of a fluorescent dye, Sanolin Rhodamine B02, in the final particulate product; this dye is selected because it sustains the operating temperatures and provides a relatively high accuracy in visible spectrophotometry. 2- a set of water dual nozzles [21] is placed at the bottom of the dryer, feeding from a water storage tank at $60\ ℃$ [20] and 3- a diversion of the slurry line [15] is installed before the nozzle arm [16], discharging into a storage tank open to the atmosphere [19].

2.2. Sampling and measurement.

Samples are taken at the exit of the tower belt [28] collecting the entire stream; they are sampled down and used for the analysis of particle size and the dye content. Size is analysed by sieving using the Taylor series from $150\ \mu m$ to $3350\ \mu m$, and the dye content is determined by the use of a UV/Visible spectrophotometer (Shimadzu UV-2401PC) at the maximum absorbance wavelength, $565\ nm$, with reference to a blank control solution. The morphology of each size class is analyzed using Scanning Electron Microscopy (Hitachi TM1000) and the distribution of the tracer within the granule is studied under optical microscopy (Leica MZ16 A). The droplet size during atomization is obtained from laser diffraction measurements (Malvern Spraytec Particle Sizer, RTSizer 5.6) of sprays made using an external rig that replicates the operation of the industrial scale unit. The droplet size distribution and the spray angle associated to the operating conditions given in Table 1 are measured from several spray durations between 1 to $2\ s$.

The walls are monitored at the inspection doors depicted in Figure 2. During steady state operation, the net initial

deposition rate is measured at six different wall inspection surfaces. The amount of material deposited from between 10 to $15\,min$ is taken, starting with a clean surface each time. Figure 2 shows that not all locations show similar rates, or the same type of deposits. The material deposited above the nozzle contains high moisture levels but the initial net deposition rate, $r_{d,o}$, is small and deposits are thin. Moving down, the deposits become drier and more brittle, until the bottom end where no significant deposition occurs. The sections nearby the nozzle show the highest levels of deposition. These are the areas where the hollow spray cone projects onto the wall (see the projection area according to the spray angle in Figure 2). Here multiple droplets with high inertia impact the deposits, generate the outer layers and cause large pieces to detach, flowing downwards close to the wall (Hassall 2011). This particular location is monitored separately, see level $4.5\,D$ in Figure 2. A dismountable plate has been designed to be flush with the inner wall of the cylinder, such that a section of the wall can be, in effect, extracted, weighted and placed back in position at different times.

3. The renewal of particulate multi-layers.

3.1. Description of air-borne and wall-borne states.

The deposits may be regarded as a continuous structure that is different from the particles flowing in the air. The material within the exit powder can therefore possess a wall or air-borne origin according to whether it has been at any point part of the structure fixed at the wall. On these bases, the dryer may be defined by the two different regions depicted in Figure 3a: a) the air-borne region comprised by the air vortex that contains a population of air-borne particles, and b) the wall-borne region comprised by the deposits that remains fixed. Both are described in Figure 3b as spatially distributed reactors where the solids undergo different transformations. In the air-borne reactor they dry, aggregate and flow, and in the wall-borne reactor, particles dry and may sinter but remain fixed. Both regions interact by a mass flow rate of particles that move from an air to wall-borne state and vice versa by deposition, r_d, and re-entrainment, r_e. In reality, these rates are distributed through the height of the tower and vary according to the local drying conditions, the deposit properties and the local rate of impacts onto the wall.

3. 2. Outline of the tracer experiments.

Decoupling experimentally the wall and air-borne processes requires determining the exchange rate between both reactors in Figure 3b and the particle residence time in each. This work studies only the wall-borne reactor, for which it is important to quantity the average rate of re-entrainment r_e and the time the particles spend resident in the deposits. These data have been generated by tracking the release of the material contained in the wall-borne reactor during a full renewal cycle, in the same way “wash-out” tracer experiments do in chemical reactors (Levenspiel 2004). In the real dryer, the requirement is to ensure at a given point in time that the material borne at the wall contains a known tracer concentration while that in air-borne state contains none. Several stages will be followed to achieve this. Initially, the unit will be brought to a standard production rate in order to generate a stable layer of deposits, at this point untraceable. Then, the dye solution will be injected such that atomised droplets have certain dye content and deposition and re-entrainment at the wall produces layers of traceable material. The unit will then be emptied of air-borne particles leaving behind a set of traceable deposits. At this point, atomization will be restarted with all droplets containing no tracer. The rate of release of the dyed material from the walls is then quantified by measuring the amount of tracer exiting in the product. In this way, the origin of aggregates can be determined, differentiating those that are generated from re-entrainment of material at the wall (dyed) from those with a pure air-borne history (white).

This experimental sequence is illustrated in Figure 4 and detailed below. The steps are designed to preserve at all times the operating conditions in the tower and maintain the properties of the deposits.

3.3. Generation and tracking of a set of active wall deposits. Sequence of a “wash-out” experiment.

3.3.1. $P-0$. Start up: The rates of slurry and hot air ramp up in order to heat the unit and develop an initial layer of

deposits associated with the particle-wall contacts.

3.3.2. $P-1$. Production: Production is carried out in steady state. The product is characterised and the multi-layer structure of deposits is formed at the walls.

3.3.3. $CH-1$. Changeover. Connection of the dye injection: Homogeneous mixing of the slurry and the dye is ensured by placing the injection before the hammer mill in Figure 1. However the long residence time between the injection point and the nozzle (from [12] to [17] in Figure 1) causes a certain axial mixing of the tracer in the slurry line. Two requirements need careful consideration, a) deposits tractability: a sharp step change in dye content at the nozzle is necessary to ensure only droplets of known concentration, either the target or zero are produced, and b) deposits mechanical properties: the mechanics of deposition and erosion is the aim of the experiment, and thus the properties of the deposits should be maintained. According to these two objectives, the following sequence is executed:

- The dye injection starts and the following two changes are executed simultaneously.
- The slurry line is diverted to an external loop connected to the atmosphere, where it discharges into a container for visual inspection, [19] in Figure 1. After this, the nozzle arm itself is purged in [18] with water vapour to avoid solidification and the blockage of the line.
- Hot water is diverted into a pair of dual nozzles in [21]. Both spray a fine water mist into the conical region, with a combined rate set to match the evaporation rate when the slurry nozzle is in operation.

In operation most of drying occurs at the bottom of the chamber. As the evaporation rate is kept constant with the use of the water nozzles, the air operating conditions can be left unchanged and in this way, the deposits in the cylinder are subject to similar air temperature, humidity and velocity at all times. Nonetheless, in certain areas the deposits are likely not in equilibrium, but slowly drying so to minimise any change in their properties, the length of $CH-1$ was reduced as much as possible. Visual inspection and analytical measurements from [19] confirm the point when the tracer achieves a target constant concentration in the slurry. At this point, the line is ready to diverted back into the tower.

3.3.4. $P-2$. Production. Generation of traceable deposits: The water flow is stopped in [21] and simultaneously, the slurry containing the target tracer concentration is diverted back from the external loop in [19] to the atomizer in [17]. All settings, including the burner, mixers, pumps and temperature control remain unchanged, and thus the atomization pressure and subsequently the droplet size, returns almost instantaneously to the steady state values of $P-1$. Production resumes and the exit powder in [28] and [26] starts showing the colour derived from the dye. This continues for $\sim 1h$, what will be proven sufficient to ensure that active layers in the deposits have been renewed and are now comprised of the traceable material. In the last $5\ min$, product is sampled tor characterization.

3.3.5. $CH-2$. Changeover. Disconnection of the dye injection: At this point the air-borne and wall-borne reactors in Figure 3b are both full of dyed particles. In order to track the material exiting the wall-borne reactor one needs first to empty the air-borne reactor and then ensuring that the new population of incoming droplets contains no dye. In order to do this, the same changeover is executed, but in this case proceeding to the disconnection of the dye. The slurry is diverted out of the tower into external container [19] and instead the water is connected. The slurry loses the colour and analytical measurements from [19] confirm the point when the dye concentration is $< 1\ \%$ of the target.

3.3.6. $P-3$. Production. Renewal of the wall deposits: At this point the reverse changes are made. The water flow is stopped and simultaneously the slurry which now contains no dye is diverted back to the nozzle in [17]. At this precise point in time, the tower is empty, the entire mass of deposits contains a given concentration of tracer and the entire population of air-borne droplets contains none. This situation is equivalent to setting a target tracer concentration in the

material within the wall-borne reactor in Figure 3b, whilst the air-borne reactor is empty. When atomization restarts, the tower fills up, and samples are taken in [28] for a period of $\sim 1h$, in such a way that the presence of the dye reveals the contribution of the re-suspended material to the product.

3.4. A note in the solid hold up and the correct conditioning of the deposits during changeovers.

The potential disruption of the deposits during the changeovers could be recognized by three signals: 1- visible changes in their morphology, 2- product exiting the tower belt or the cyclones or 3- stagnation of solids hold up in the air. The inspection of the wall is discussed in section 4.3, showing no significant changes during the changeovers. In addition, no powder was seen to exit the unit in these periods. No powder exited from the tower belt, which indicates that detachment of large pieces due to gravity is not significant and at the cyclone exit, a negligible flow was observed.

At the end of $CH-1$ the tower is assumed to be empty, but it might have contained solids stagnated due the counter flow. Evaluation of this is essential to keep the tractability of the deposits (i.e. ensuring that when the atomization restarts in $P-3$ the only particles in the unit that contain the dye are borne at the wall). This has been confirmed in a separate experiment. The same sequence was repeated but in this case, at the end of $CH-1$ the water nozzles and the air system were both shutdown simultaneously. The solids hold up exited through the tower belt and were collected. The amount represents $< 0.4\ \%$ of the weight of the deposits and a negligible concentration in the dryer. It is noticeable that after $25\ min$ of the shutdown, a larger section of the deposits detached (4.5 % of the full weight). This highlights the impact that the air conditions have in the deposits properties, and the success of this sequence in preserving them.

4. Results and Discussion.

4.1. Transient production.

When the unit fills up in $P-3$, the mass rate of powder exiting from the bottom, denoted M_P, increases before reaching its steady state value, $M_{P,St}$. This evolution was determined in a separate experiment. The same sequence was replicated and when the atomization restarted in $P-3$, M_P was measured manually. Figure 5a presents the evolution of both the rate and the product size distribution in $P-3$. It is clear from both that it takes $\sim 100\ s$ for the unit to fill and achieve the steady state concentration. This is in agreement with the particle air-borne residence times $< 30-45\ s$ reported for similar units by Harvie *et al.* (2002) or Huntington (2004) and more recently for the same spray dryer in Ali *et al.* (2013) or Ali (2014). The initial size distribution is very narrow and contains primarily the size fractions that later become the mean product size between $300-600\ \mu m$. As time progresses, the distributions span and start containing a larger proportion of small and large sizes, stabilizing close to the steady state average at $t > 100\ s$. It is a noticeable fact that both, larger and smaller size fractions take longer to exit, since one expects the large granules to sediment faster. This could be explained by the fill up, if large aggregates are formed only when particle concentration rises sufficiently. However, it is most likely related to a high level of interaction with the walls, discussed in detail later.

4.2. Steady state production.

Figure 5b compares the size distribution of the droplets and the product in stages $P-1$, $P-2$ and $P-3$. The atomization covers a range from $20-1000\ \mu m$ and is skewed over the large sizes, having a mode from $350-450\ \mu m$, a median volume size of $x_{p,50}$ = 292 μm, and 10th and 90th percentiles, $x_{p,10}$ and $x_{p,90}$ of $85\ \mu m$ and $512\ \mu m$ respectively. The product undergoes a significant particle growth, the distributions covering a range from $70-10000\ \mu m$. They all present a mode between $300-400\ \mu m$, a median mass size $x_{p,50}$ ranging from $360-430\ \mu m$ and $x_{p,10}$ from $160-180\ \mu m$. From the early stages in $P-1$ the product size distribution in Figure 5b shows a long tail $> 1000\ \mu m$. However, as the time progresses in $P-2$ and in $P-3$, the tail becomes more significant and $x_{p,90}$ varies from $1350\ \mu m$ in $P-1$ to $2540\ \mu m$ in $P-3$. Stable operating conditions are reached

in all cases, including relatively constant heat losses in the dryer. However, the product size evolves during a period of $\sim 2-3\ h$, which is much higher than the residence times involved in particle flow. This indicates that during the initial stage, processes other that fluid dynamics must still be in a transient state. The next section associates this effect with the stabilization of deposition and re-entrainment rates.

4.3. Deposition and re-entrainment equilibrium.

Figure 6 presents photographs of the extractable plate located at the wall in the level $4.5\ D$ taken during the entire experiment. In parallel, Figure 7 provides the evolution of the weight of the ensemble (plate plus deposits) associated to the same images. In the start-up, $P-0$, deposition increases until the product covers the entire surface. During this period, the weight of the deposits rises linearly in Figure 9, at a constant net deposition rate, $r_{d,o} = 111\ gmin^{-1}m^{-2}$. After this stage, the weight on the plate stabilizes. No significant variations can be related to either of the changeovers, which indicates that the mechanical properties of the deposits have been kept within reasonable margins. The tendency to achieve a maximum weight or thickness, where the net deposition rate falls close to zero is a common observation in particulate fouling known as the 'blocking effect' (Henry *et al.* 2012). In cases of low inertia and cohesive forces it is in part related to re-entrainment and in part to the suppression of deposition.

A similar evolution was reported by Hassall (2011) working in swirl spray dryers at higher cohesive forces and particle inertias, but until now its root cause remained unclear. Figure 9 shows that when the spray varies from white to dyed to white again, from $P-1$, $P-2$ and $P-3$, a change follows in the colour of the deposits. This confirms there is deposition of atomized droplets. But further on, as the colour change occurs, the weight of the ensemble given in Figure 10 remains constant. This is a major and important result: it provides the first experimental evidence of significant wall dynamics in these units. It demonstrates that the rates of deposition r_d and re-entrainment, r_e are in equilibrium in this section, and that such a renewal process is responsible for suppressing the growth of the deposits. Notice that they change sharply in colour, not gradually and thus the structure must be renewed quickly. New sets of clusters must be brought from the air into the structure to be re-entrained back into an air-borne state a given time later.

4.4. Quantification of the re-entrainment rate.

The detergent slurry contains three different phases, and it is noted that the dye used in this work distributes preferentially within the organic phase and therefore, dye and surfactant contents are correlated. The surfactant/s level in the product varies across different sized particles, primarily for the sizes $< 212\ \mu m$ (Francia 2014a), and accordingly, pure dyed particles present a similar variation. For this reason, the reference dye content was obtained for each size class using the pure dyed powder obtained at the end of -2 . X is defined in (1) as the ratio between the dye content of a mixture and that of the pure dyed powder of the same size range, for a given sampling time t.

$$X_{s,t} = \frac{S_{s,t} \cdot A_{s,t}}{S_{s,ref} \cdot A_{s,ref}} \qquad (1)$$

X is equivalent to the ratio of dyed material present in the mixture. Notice that during $P-3$, the dyed material has a single possible origin: the deposits, and therefore X is equivalent to the ratio of material that in fact, has a wall-borne origin, i.e. the material that was part of the deposits and was re-suspended after the atomization starts in $P-3$. The use of (1) carries a certain error when the deposits have a different content in surfactant/s or tracer than the product. All the data reported here include a largely conservative estimate of this uncertainty.

Figure 8 presents the evolution of X for all size fractions in the samples taken during $P-3$. At the initial time, $t_0 = 0\ s$, the entire mass of deposits is dyed and the entire population of air-borne droplets is white. At that point, the exit rate of dyed material, denoted X_o, can be considered an estimate of the instantaneous re-entrainment rate r_e. The

first re-entrained material is simply delayed a given time before exiting due to the air-borne flight between the re-entrainment position and the exit. Within the initial $100\,s$ (i.e. the filling up period) the mass averaged value of X decreases from an initial value X_o of $20 \pm 1\,\%$ to $12 \pm 1\,\%$ of the full production rate. This range increases to values between $31 \pm 1\,\%$ and $15 \pm 1\,\%$ for the mass fraction $< 212\,\mu m$ and up to a range between $37 \pm 3\,\%$ and $10 \pm 1\,\%$ for the mass fraction $> 850\,\mu m$. At times $t > 0\,s$, the deposits and the re-entrained granules start containing white material, deposited between t_0 and t, which makes X to diminish. However, the initial sharp decay is more likely related to fast time scales in the renewal process. Notice that any deposition and re-entrainment cycles that occur faster than the first sampling time $\sim 15\,s$, would blend in with the air-borne material, appearing as white in the product. On this basis, the ranges given are minimum estimates of the removal, because the fastest interactions are not included.

These observations have major implications to the general view of the behaviour of swirl counter-current spray dryers. In a detergent context, a significant fraction of the product, $> 12\,\%$ and most likely $> 20\,\%$, is not material originated at the nozzle but is material generated from the wall deposits and its size, structure and drying history is related to the physics governing fouling (i.e. deposition, ageing and erosion of a network of clusters). These values become even more relevant for smaller and larger aggregates, known to have higher water contents and a significant impact in the energy balance (Francia 2014).

4.5. Granule structure and morphology.

Figure 9 provides some examples of the morphology observed under SEM analysis, and Figures 10 provides examples of analysis of the exit powder under optical microscopy. Figures 10a and 10b provide micrographs of the product exiting at the average mode age determined later as $t \sim 157.5\,s$ and at the initial sample $t \sim 7.5\,s$, and Figures 10c and 10d provide details on the structure of the mixtures between air-borne droplets and wall-borne clusters. A collection of micrographs is available in the supplementary material.

4.5.1. Small and average size particles $< 850\,\mu m$.

Lower size fractions shown in Figure 10a are comprised, in general terms, of pure particles, either completely white or dyed. Several observations follow. Firstly, the history of pure dyed particles must involve no aggregation with any air-borne droplet. This includes 1- the time they had remained wall-borne, potentially sintering with newly deposited droplets or subject to impacts, 2- the contact with other particles during the re-entrainment mechanics itself, and 3- the air-borne history from re-entrainment to exit. Secondly, despite the fact that no aggregation occurs, the detachment has been triggered by the impacts of air-borne particles. No particles exit during the changeovers nor are they hold up in the air when tower is empty and the deposits are subject to the same stresses due to gravity or aerodynamics.

The re-entrainment of pure dyed particles must follow two potential mechanisms, discussed in more detail in section 5. First, the impacts of dry particles causing a direct detachment: in this case, both, particles and deposits are dry enough not to develop sufficient adhesive forces and cause deposition or capture, but the impacts contain a large enough inertia to break the bonds between the clusters. Second, the detachment of large pieces: being typically of a low density and heterogeneous shape, large clusters are unlikely to retain their shape and break down into smaller particles (Hassall 2011). The detachment of large pieces can be triggered by the action of gravity alone or combined with the impact of dry particles or wet droplets. Note that the breakage of individual bonds in the multi-layer structure can, in combination with gravity, lead to detachment of a large section.

4.5.2. Large particles > 850 µm.

The morphology of the large granules is itself heterogeneous, see Figure 9. In general, they present a variety of

non-spherical structures and a high aspect ratio. Primary particles appear to be fused together forming granules with wide cavities, comparable in size to the primary particles that they contain. When particles collide between each other or to the wall, such surface features surely lead to a very different behaviour from spheres, especially with regard to interlocking and rotation. Figure 9 includes several examples showing a clear heterogeneity in particles having smooth and aggregated sides. This feature could be explained by the interaction with the wall. In a two dimensional multi-layer, sides can be exposed or not to sintering, and subject or covered from air-borne collisions.

In large granules the wall-borne, or dyed, material is distributed in a different manner. In part, they are also comprised of identifiable pure dyed particles, which indicates the presence of a similar production mechanism as for the smaller particles. However, the remaining particles are not purely white but, as illustrated in Figure 10b they are in general mixtures of air-borne and wall-borne material. Figures 10c provide examples of the external distribution of dye, where the graduation in the colour intensity at the surface results from an outer layer of white material, varying in thickness. Aggregates range from pure dyed particles to white granules with coloured sections, where dyed primary particles are embedded in the granule. As the time progresses the deposits turn white and mixed granules containing only small sections of coloured material become common. However, the largest fractions still contain $> 10\ \%$ of dyed material after the tower has been filled (i.e. $\sim 100\ s$), which indicates the dye is still present in the inner structure of the granule. Figure 10d shows how large granules vary from homogeneous mixtures containing multitudes of white and dyed primary particles, to granules where a dyed wall-borne nucleus is captured by white air-borne material.

This analysis demonstrates that wall-borne clusters undergo aggregation with atomized material. This is a revealing fact. It indicates that the production of most large aggregates in the product is driven by the dynamics established at the wall. In this sense, the re-entrainment rates given earlier should be taken as an indication of the mass that is re-entrained from the deposits and exits within large individual granules, but noticing that in fact, most if not all of these particles are affected by the cycle of deposition and re-entrainment. Aggregation might occur at the wall, or close to it after the material has been re-entrained. However it is worth noticing that the recirculation of solids from the wall into the proximities of the nozzle is very unlikely. Due to the swirl particles migrate outwards; most of them flow down close to the wall and the smallest particles are recirculated up, but turbulence is no sufficiently strong to disperse them inwards, what occurs only near the top end. This, in addition to the lack of mixtures observed $< 850\ \mu m$ suggests that the recirculation is not likely to be the responsible of the generation of the mixtures shown in Figure 10. Section 5 discusses in detail other aggregation mechanisms linked to the re-entrainment mechanics.

In conclusion, the manner in which the wall-borne material distributes in the exit granules is correlated with their size. Small and average sizes are in general terms re-entrained as pure aggregates. Large size classes can also be re-entrained directly but in the majority of cases the process involves the aggregation between wall clusters and air-borne droplets.

4.6. Residence time of the re-entrained material.

The age distribution, AD, of the re-entrained material can be quantified by measuring the exit rate of dyed material in $P-3$ at the intervals defined by the sampling times, similarly to a “wash-out” type of experiment (Levenspiel 2004). Samples cover the full renewal cycle of the deposits in $\sim 1h$. The average exit rate of wall-borne material is denoted w and given in (2) for the size class s and time interval i between the i^{th} and i^{th-1} samples. It is function of the exit mass rate, M_P, and the ratio of material of wall-borne origin, X, given in Figures 5 and 8. A standard age probability density function, E, is estimated in (3) normalizing w by the total re-entrained mass, W. The latter is obtained in *(4)* for each size class s by the integration of w during the entire renewal process comprised of n samples.

$$w_{s,i} = \frac{1}{2}\left(M_{P,s,i-1}X_{s,i-1} + M_{P,s,i}X_{s,i}\right) \quad (2)$$

$$E_{s,t} = \frac{w_{s,t}}{W_s} \quad (3)$$

$$W_s = \sum_{i=1}^{n} w_{s,i} \cdot (t_i - t_{i-1}) \quad (4)$$

Note that E is not in strict terms the product residence time distribution, RTD. It is the exit age distribution, AD, of the material borne at the wall after atomization restarts. It includes the residence time that it takes for a granule at the wall to be re-entrained, plus its air-borne residence time to the exit. In order to facilitate the comparisons across the different size ranges, E are normalized in (3) by the mass re-entrained within each fraction, W_s. The whole set of functions provided in Figure 12 can be interpreted directly as the probability of the material that is re-entrained within a given size range s to exit at a given time t. Logarithmic plots allow a better visualization when the distributions present very long tails. For this reason, a density function, E_{log}, based on a logarithmic time is also calculated in (5).

$$1 = \int_0^{\infty} E_s(t) \cdot dt = \int_0^{\infty} E_{log,s}(t) \cdot d(logt) \quad (5)$$

The mean or average residence time $\bar{t}$ is given as the first moment of E is provided in (6).

$$\bar{t}_s = \int_0^{\infty} t \cdot E_s(t) dt \quad (6)$$

Table 2 summarizes the statistics of E. A characteristic mode occurs between the samples at $157.5\,s$ and $247.5\,s$, while t_{84} ranges from 1350 to $1720\,s$ depending on the size of aggregates. The median age t_{50} and the mean $\bar{t}$ range between $310 - 510\,s$ and $710 - 870\,s$ respectively. These values are, in average, from ten to a hundred times higher than the residence time expected from the trajectories of the air-borne particles in similar units, $< 30\,s$ (Huntington 2004, Harvie *et al.* 2002) or more recent numerical simulations in the same dryer (Ali *et al.* 2013, Ali 2014) which report much lower values for the largest particles. The large time that the particles spend at the wall may explain why current models struggle to explain how drying occurs in such short air-borne residence times.

As time progresses the relative error in E becomes higher due to the smaller concentrations of dye. The tail of the distributions prolongs for a long time and at the final part, a large section is defined by fewer samples. This lead to a higher uncertainty in w and the integration in (4) explains why the confidence intervals in t_{50} and t_{84} are larger. This is particularly relevant for the largest granules which show a secondary mode at larger times.

4.7. Time scales in the re-entrainment mechanics.

The same correlation between the aggregate size and the dye distribution appears in the analysis of the age distributions. The AD of the whole re-entrained material is compared with those of each size fraction in Figure 11. Two distinct groups can be distinguished: one is related to smaller fractions than the average product, another to large granules $> 850\,\mu m$. These are split in Figures 12a and 12b.

The smaller fractions result from the re-entrainment of pure particles and present a wide span in Figure 12a. In particular, the fractions $< 300\,\mu m$ present a secondary mode between $300 - 600\,\mu m$ and a prolonged exponential decay. As expected, fractions close to the mean sizes follow closely the average AD. The distributions obtained in the large fractions are shown in Figure 12c. As the size rises $> 850\,\mu m$, the history of the granules starts to include the aggregation of air and wall-borne material and the function changes, deviating from an exponential decay. The set of functions obtained is now clearly different from the average, and progressively narrows around the mode with increasing particle size. In addition, a secondary mode appears in all the fractions between $1100 - 1700\,s$. As illustrated by the logarithmic plots in Figure 12b and 12d, it gains relevance in the largest granules. The span of this mode cannot be estimated accurately but it is worth observing that it is the presence of this feature which modifies the average statistics of large fractions in Table 2, moving them towards larger means, comparable in all fractions. Figure

12 shows that the AD functions however have a clearly different nature.

The decrease of E given in Figure 12a could be approximated to an series of exponential decays characteristic of continuous stirred tank reactors, $CSTR$. However, these sizes exit as dyed pure particles, which discards the assumption of release from a well-mixed layer. The slow decrease here rather than mixing indicates the kinetics of the renewal. Notice that the probability of the particle impacts to re-entrain dyed clusters from the outer layers decreases with , as they renew and the surface exposing dyed sections decreases. In Figure 12c, ADs tend to be closer to an ideal plug flow reactor, PFR with axial dispersion, than they are to a $CSTR$. This indicates that again, despite being mixtures, large granules do not come from a well-mixed structure that renews gradually. This would result in the exponential decay of E, where the mixtures would be generated gradually. The re-entrainment however seems to occur at a faster time scale that produces mixtures from the first moment, which then exit with a narrow age range.

The distributions shown in Figure 12 fit well to a system of ideal reactors. In particular, the inflexion point in the average profile fits well with a system with two $CSTR$s in parallel (Levenspiel 2004). In each branch, one $CSTR$ followed by one PFR can represent the time particles spend in the deposits and the flow from the re-entrainment to the exit. A large or a small $CSTR$ in each branch can be used to approximate respectively the long or short time scales observed in the re-entrainment. However, it is important to note the limitations of such approaches. The values of E reported here are in effect an average over the entire deposits' surface, which is itself very heterogeneous, see Figures 2 and 6. Deposits are not a well mixed structures, but layers that grow in thickness and then break up. This very likely happens at different time scales in different sections because of the changes in the properties of the deposits (e.g. water content) and the stresses they are subject to (e.g. drag or particle impacts). This type of spatial effects cannot be described accurately by an ideal $CSTR$ approximation. The secondary mode in Figure 12d and the corresponding shoulder in all smaller classes in Figure 12b provide a good example. It cannot be explained by a gradual renewal of outer layers because it owes to a sharp change in the re-entrainment rate: a significant part of the deposits exit at a time scale one order of magnitude higher than the mode, and twice higher than the mean. Such a sudden change could be linked to areas of the wall dominated by shedding, or detachment of large sections. This intermittent phenomenon is a common observation in dryers (Hassall 2011) and can release a considerable mass (see section 3.4).

To sum up, Figure 12 demonstrates that re-entrainment occurs at various time scales, which are correlated with the final granule size. In combination with the morphology analysis, it appears that fast and slow time scales are associated respectively to re-entrainment of granules with and without the aggregation with air-borne material.

4.8. Exit size of air and wall-borne material.

The size distributions of air-borne and wall-borne material are compared with the initial droplet size in Figure 13. The eroded material has a higher proportion of smaller fragments but both show similar tails and distributions. Both present a clear growth pattern from the atomization to the exit. Bearing in mind that there are no particular differences in the morphology of pure particles, air-borne (white) or wall-borne (dyed), there are no evidences to suggest that they have been formed in a different way. The question remains on whether the growth occurred 1- before they were deposited, i.e. coalescence, 2- upon the deposition itself, 3- during a long time in wall-borne state or 4- after re-entrainment. Nonetheless, note that the population of pure white particles may have also interacted with the deposits but at faster time scales than the measurement, and thus the level of interaction with the wall can be higher than the reported by X. The same origin can be thought for the mixtures, with the obvious exception of having aggregated before deposition. The likelihood of the different hypothesis will be analyzed in the next section.

5. A wall dynamics framework for swirl assisted dryers.

This section discusses the most likely dynamic of deposition and re-entrainment within counter current swirl dryers, and highlight specific areas for research. An outline is provided in Figure 14, which depicts the ageing process and different contact mechanics by which the air-borne product may interact with the multi-layer structure. It considers the sources of re-entrainment associated to the action of aerodynamic forces, gravity and the impact of wet droplets and dry particles, which lead to dry and wet mechanisms of erosion, and cause the detachment and breakage of large clusters.

5.1. Deposition and contact mechanics.

Coalescence and particle/droplet impacts are largely studied at a small scale, (e.g. Qian and Law 1997, Liao and Lucas 2010) particularly in sprays (e.g. Rüger *et al.* 2000, Post and Abraham 2002), or for instance in kinetic descriptions based on the viscous and deformation Stokes numbers, applicable to granules with an elastic core and an outer binder layer (e.g. Liu *et al.* 2000, Iveson *et al.* 2001,). The contacts described in Figure 14 for a spray drying context involve higher viscous forces and different structures. Here, particles / droplets have a wide range of viscosities and show a hard outer crust and a soft core (Handscomb *et al.* 2009). Some authors approximate these collisions as the inter-penetration of viscous spheres of a constant shape (Hoeven 2008) but only recently detailed experiments have been made available by Kuschel and Sommerfeld (2013), providing validation data for advanced numerical models (Focke *et al.* 2013). The impacts to a fix substrate can be thought in very similar terms, but need to recognise the role of the microstructure, i.e. how the cohesive forces drive the behaviour of the wall-borne clusters. The time scale and the contact area developed in an impact depend on the drying state of deposits and the impacting droplet, and the impact inertia. Deposition occurs only if the adhesive force generated is higher than the aerodynamic disruptive stresses of a similar time scale, plus those from an inertial source: a) the shear stress caused by gravity and the centrifugal inertia and b) the elastic recovery which causes a normal detaching force.

Impacts between sufficiently dry partners, see stage [11] in Figure 14, result in rebound in [14]. The bonds between wall-borne clusters however need sustaining the stresses derived from the impact. If they are large enough, they may cause the breakage of the microstructure and re-entrainment in [11,12,13] detailed further in section 5.4.1, or in [11,12,5,6] detailed in section 5.4.3. Impacts develop a larger contact area when droplets are deformable in stage [1]. Two possibilities may be considered. One, deposition at low inertias in [2], where both adhesive (droplet-cluster) and cohesive forces (between clusters) sustain the impact stresses. Another, at high inertias in [8]: the larger droplets impact the wall at high velocity, which generates a larger contact area and a higher shear stress. Capture occurs when the shear stress breaks the bridges between neighbouring clusters but the adhesive forces between the droplet and the cluster can sustain it, see stages [1,8,9] or [1,8,5,6,7] in Figure 14. This sort of wet erosion is detailed in section 5.4.2 and 5.4.3.

Other factors such as wall roughness and particle shape play an important role. The balance of forces at the contact depends greatly on the disposition of the roughness (Guingo and Minier 2008) and the sole action of the heterogeneities owed to the deposits has an important effect in particle flow and residence time (e.g. Sommerfeld 1992; Sommerfeld and Huber 1999). Consider that in this case the surface features of the clusters at the wall are very large, comparable to the cavities of impacting particles, if not the particles themselves, see Figure 9. In addition, elutriated fines contain many ligaments produced during atomization, which appear as coiled structures in the product, see Figure 15. In this context, particles can get trapped at the wall by simply locking or rotating in the cavities of the outer layers. This would increase significantly the residence time and may explain the difference between the mode residence time of the large r-entrained granules in Figure 12c (between $157.5 - 247.5\ s$) and the air-borne residence time expected from models.

5.2. Ageing.

The particle-particle forces at the deposits evolve as time progresses in stage [3]. New bridges are formed by deposition

in [2] and [10] and the existing ones solidify, becoming more porous and brittle (e.g. Tardos and Gupta 1996; Farber *et al.* 2002; Bikaa *et al.* 2005). In addition, as the layer grows, the clusters start containing higher numbers of primary particles but are sustained by a lower specific contact area, which facilitates their removal due to gravity.

The evolution of contacts such as those shown in Figure 15, responds to the rates of different transport phenomena, some of which are described by Wang and Harb (1997) for the erosion of ash deposits. On one hand, external heat and mass transfer rates dry the structure, increase its porosity and accelerate the crystallization of salts, and on the other hand, large differences in the water content facilitate the migration of species. These are long time scale processes that occur in parallel with the momentum transfer driven by impacts, the action of the Laplace pressure and gravity. Their combination ultimately determines the sintering rate. It is important to advance in the evaluation of the relative time scales of these phenomena because properties such as viscosity or water diffusion coefficients vary across several orders of magnitude as the material dries at the wall. Ultimately, the time it takes for the viscous-like material deposited to turn into a deformable solid will constrain the rate at which the bridges can thin or sinter.

5.3. Origin of the disruptive stresses.

The multi-layer at the walls breaks when it cannot sustain the stresses caused by the inertia of the impacts, gravity and the drag and lift forces caused by the air flow. However, it is interesting to note that when the tower is empty, re-entrainment stops (see section 3.5). Thus the particle impacts must be necessary to trigger it. This can be explained by 1- outer layers growing sufficiently so that gravity cause the detachment in stages [2,3,4,5,6] in Figure 14, or 2- breakage due to the impact of dry particles in [11,12,13] or wet droplets in [1,8,9]. In each case, re-entrainment occurs at very different time scales: 1- a long one occurs after deposition, aging and shedding so that the size of the re-entrained cluster is related to the microstructure of the multi-layer, and 2- a short one occurs as a result of impacts, and thus the size of the re-entrained cluster is also related to the properties of the particles or droplets responsible.

In stage [6], gravity and aerodynamic forces alone may suffice to induce the removal of clusters when they grow. Now, this implies the aggregation between new droplets and the wall-borne clusters, and as such, we should expect the product to be comprised in general of mixtures. Indeed, this occurs for the large granules but it does not for most of the product. The next section discusses several re-entrainment mechanisms that can explain this behaviour.

5.4. Mechanisms of re-entrainment.

The material bounded at the multi-layer exits the unit in two different populations: 1- A set of granules is re-entrained directly with no aggregation and at a long time scale, and 2- Another set, $> 850\,\mu m$, is comprised of aggregates of wall-borne clusters and air-borne droplets and exits at much shorter time scale. Both show intermittencies.

5.4.1. Dry mechanisms of erosion.

Multiple impacts of dry particles with sufficient inertia to break bonds within the structure of the deposits causes the direct re-entrainment of aggregates, as depicted in [11,12,13] in Figure 14. In combination with gravity it may be also be responsible of triggering the detachment of larger pieces and their subsequent breakage in stages [11,12,5,6,7]. This type of contact is associated with both, drier particles and drier sections of the multi-layer (above and below the projection of the nozzle in Figure 2). In this case, re-entrainment occurs as a single event and for this reason, one may associate the long decay in E in Figure 12a to the time that particles remain fixed at the wall rather than to the time of flight between the wall and the exit.

The lack of mixtures is noticeable. Pure re-entrained particles do not appear to have sintered with the newly deposited material, which has two possible explanations. One is that drying fixes their size after deposition and this suppresses sintering. This suggests that growth occurred before the time at the wall, e.g. during coalescence, or at the deposition

impact itself. Another explanation comes from the production of pure particles by breakage in stage [7]. In this case, the largest granules are more likely to survive containing the mixed regions, leaving smaller particles pure.

5.4.2. Wet mechanisms of erosion.

A part of the re-entrained deposits exits after having aggregated with air-borne material and presents a clearly different residence time. The mixed granules must be produced by 1- aggregation upon the deposition of new droplets, 2- sintering in a wall-borne state or 3- contacts after the erosion. The latter implies coating after numerous impacts with small droplets or the capture by large ones. Both are very unlikely given the low concentrations away from the wall (Hassall 2011). In regards to sintering, it may be responsible of the formation of solid bridges, but it does not generate the mixtures because they exit not only at large times but from the first moment.

The most likely origin for the mixtures is direct growth upon the impact of wet droplets in [8] in Figure 14. These present the largest inertia and are common in the area of the spray projection. Here droplets $> 200\,\mu m$ still have high water contents and momentum when they impact the wall, which occurs at tangential angles $< 10\,°$. Upon colliding, they deform, lose energy due to viscous dissipation and capture aggregates, either in close proximity to the wall or already bounded at the structure. Stages [1,8,9] in Figure 14 describe a rolling mechanism whereby wall-borne clusters act as initial rigid nuclei that becomes encapsulated. This appears as a likely contact mechanics in agreement with the morphology observed and similar “Rock´n Roll” mechanisms proposed for re-suspension of single particles (e.g. Vatistas 1992; Reeks and Hall 2001 or Zhang *et al.* 2013). Newly formed encapsulates may deposit in [10], roll or saltate along the surface, or become detached in [9]. If rolling or saltation occurs, the granule may keep picking up clusters in a snowball effect. Its ability to grow would quickly decrease as the surface dries and the inertia dissipates.

As opposed to dry erosion, re-entrainment now is comprised of multitude events occurring at fast time scales. For that reason, the mode in Figure 12 can be thought to be related not to the time in a wall-borne state, but rather to the air-borne history which is obviously affected by numerous contacts with the wall. The mode residence time reported may be related to the saltation of granules documented before in the same dryer (Hassall 2011). They may indicate the time it takes for wet large granules, initially formed close to the nozzle projection, to saltate down the surface of the chamber, growing as they come in contact with the wet areas of deposits.

5.4.3. Shedding and breakage.

Deposits in Figure 6 show large variations in thickness, and identifiable groups of clusters at the surface. This is the result of a shadow effect (i.e. the heterogeneity of the outer layer makes particles to pile onto the same area rather than distribute homogenously). This is emphasized in this case by non-spherical shapes and the low impact angles to the wall.

As the clusters grow, they become destabilized and can detach in stage [6]. As described before, shedding may be triggered directly by the growth of the layer or by the impact of particles / droplets at high inertia in [5]. Once large pieces are detached, they are not likely to sustain the stresses in an air-borne state and break down into smaller fragments in [7] which contain both, pure particles or mixtures depending on whether the initial impact involved wet droplets or dry particles in [8,5,6] or [12,5,6] or both if the detachment was purely triggered by gravity in [4,5,6,7]. The presence of these intermittent events may explain the largest time scale features observed in the age distributions.

Conclusions.

This work demonstrates that the wall dynamics can have a major impact in swirl counter-current spray dryers:

a) Rate. In the context of detergent manufacture, deposition and re-entrainment are found to be in equilibrium for the most relevant section in the dryer. The re-entrainment rate comprises $> 12 - 20\,\%$ in mass of the full production,

becoming higher for both smaller size fractions and particularly aggregates $> 850\ \mu m$ in diameter.

b) Time scale. The mechanics of re-entrainment varies for aggregates of different size. Small and average size particles are directly re-entrained with no aggregation with air-borne material. In contrast, aggregates $> 850\ \mu m$ appear as mixtures of both and thus are almost entirely originated in cycle of deposition and re-entrainment. However, no differences are appreciated between the morphology of pure re-entrained particles and the rest. Bearing in mind that the re-entrainment rates given are under predictions, the level of interaction with the multi-layer may be much higher. The time scale of this equilibrium has also an important effect in the residence time of the product, thus affecting its drying. The material undergoing the wall cycle has a residence time ten to a hundred times higher than the values expected from their air-borne trajectories. Such a large deviation represents a serious handicap in numerical models, which neglect the largest proportion of the time that the re-entrained product remain exposed to heat and mass transfer rates.

c) Growth and Structure: Different re-entrainment time scales have been identified as the responsible of producing re-suspension of deposits either with or without the aggregation with air-borne material. These have been correlated respectively with the generation of most of the aggregates $> 850\ \mu m$ and a fraction of the smaller and averaged sized particles. Accordingly, a series of mechanisms has been proposed to describe this process. They include the re-entrainment caused by the impact of dry particles, capture and aggregation caused by the impact of wet droplets, and their combination with gravity to cause the detachment of large clusters and their breakage.

In summary, this work highlights the relevance of deposition, ageing and re-entrainment in swirl spray dryers. Their effect goes beyond prior considerations, dominating the drying kinetics, the particle growth and the structure of a significant proportion of the product, at least under detergent manufacture. Numerical models based exclusively in the description of the fluid dynamics and particle processes during their flight in the dryer not sufficient to describe the process. Addressing this limitation implies being able to describe the structure of the deposits and the mechanics governing its renewal. This could led to a better control of re-entrainment rate and the product properties, for instance adjusting operating conditions such as the swirl intensity, the flow kinetic energy or the slurry formulation.

Acknowledgments.

VF was supported by an Engineering Doctorate Studentship sponsored by the Engineering and Physical Sciences Research Council (EPSRC) and Procter & Gamble in the Industrial Doctoral Centre in Formulation Engineering, School of Chemical Engineering, University of Birmingham.

The authors thank Mr. Andrew Roberts, Mr. Dave Banks and the tower operation crew at P&G in Newcastle upon Tyne for their commitment in the coordination and execution of the experiments.

Nomenclature

A	Absorbance, -.
D	Tower diameter, m.
E	Age probability density function, s^{-1}.
H	Distance from air inlets to vortex finder, m.
M_P	Total mass in the wall plate , kg.
M_P	Product mass rate from the tower belt, kg s^{-1}.
M_E	Mass rate of elutriated powder from the cyclones, kg s^{-1}.
S	Dilution factor , $m^3 . kg^{-1}$.

T	Temperature, °C.
W	Dyed material exited in a given time and size range, kg.
X	Ratio of wall-borne material, -
d	Diameter of the vortex finder, m
f	Size frequency, $\log(\mu m)^{-1}$
r	Mass rate, $kg.s^{-1}$
t	Time, s.
w	Exit rate of dyed material (wall-borne material), $kg.s^{-1}$
x_p	Particle diameter, µm.
z	Distance to the air inlets (m).

Subscripts

IN	For the inlet air line
EX	For the exhaust (exit) air line
A	For the air
P	For the product exiting from the tower belt
S	For the slurry
d	Deposition.
e	Erosion.
$cone$	At a location in the conical section of the drier
final	At the average of the steady state period.
log	Based in the logarithm of time t.
max	Upper side of an interval
n	Time range
t	At time t, or in sample at time t.
o	Initial or at the initial sample.
ref	For the reference obtained on $P-2$
s	Size fraction.
St	At the steady state.

References

Ali M., Mahmud T., Heggs P.J., Ghadiri M., Francia V., Bayly A.E., Djurdjevic D., Ahmadian H., Martin L. (2013). CFD modeling of a counter-current spray drying tower. International conference in multiphase flow.Jeju, South Korea.

Ali M. (2014). Numerical modelling of a counter-current spray drying tower. PhD thesis. University of Leeds. Leeds. United Kingdom.

Bashir M.S, Jensen P.A., Frandsen F., Wedel S., Johansen KD.,Wadenbäck, J., Pedersen S.T. (2012). Ash transformation and deposit build-up during biomass suspension and grate firing: Full-scale experimental studies. Fuel processing technology, 97, 93-106.

Bikaa D., Tardos G.I., Panmaia S., Farbera L., Michaelsa J. (2005). Strength and morphology of solid bridges in dry granules of pharmaceutical powders.Powder Technology. 150, 104-116

Dubrovsky V.V., Podvysotsky A.M, Shraiber A.A. (1992) “Particle interaction in three-phase polydisperse flows” International journal of multiphase flow, 18, 3, 337-352.

Epstein N. (1983). Thinking about heat transfer fouling: A 5x5 matrix. Heat transfer engineering, 4, 1, 43-56.

Farber L., Tardos G.I.,Michaels, J.N. (2003). Evolution and structure of drying material bridges of pharmaceutical excipients: studies on a microscope slide. Chemical engineering science, 58, 4515-4525.

Francia V. (2014). Spray drying of detergents in counter current towers: A study if turbulent swirling flows, fouling and agglomeration. EngD Thesis. School of Chemical Engineering, University of Birmingham, Birmingham, UK.

Francia V., Martin L., Simmons M.J.H., Bayly A.E. (2014a). An experimental investigation of the swirling flow in tall-form counter-current spray driers. Submitted to Journal of Fluid Mechanics.

Francia V., Martin L., Simmons M.J.H., Bayly A.E. (2014b). Operation regimes, wall friction and scale up criteria in tall-form swirl pray driers. Submitted to AICHE Journal.

Focke C., Kuschel M., Sommerfeld M., Bothe D. (2013). Collision between high and low viscosity droplets: Direct Numerical Simulations and experiments.International journal of multiphase flow, 56, 81-92.

Guingo M. and Minier J.P. (2008).A new model for the simulation of particle resuspension by turbulent flows based on a stochastic description of wall roughness and adhesion forces. Aerosol Science, 39, 957-973.

Handscomb C.S., Kraft M., Bayly.A.E. (2009).A new model for the drying of droplets containing suspended solids.Chemical engineering science, 64, 628-637.

Hanus M.J. and Langrish T.A.G. (2007a).Re-entrainment of wall deposits from a laboratory-scale spray dryer. Asia-Pac. Journal of chemical engineering, 2, 90-107.

Hanus M.J. and Langrish T.A.G. (2007b).Resuspension of wall deposits in spray dryers. J. Zhejiang University Science A., 8, 11, 1762-1774.

Harvie D.J.E., Langrish T.A.G., Fletcher D.F. (2002). A computational fluid dynamics study of a tall-form spray dryer.Trans IChemE, 80, Part C, 163 - 175.

Hassall G. (2011). Wall build up in spray driers. EngD Thesis. School of Chemical Engineering, University of Birmingham, Birmingham, UK.

Henry C., Minier J.P., Lefevre G. (2012). Towards a description of particulate fouling: From single particle deposition to clogging. Advances in colloid and interface science, 185-186, 34-76.

Hoeven M.J. (2008). Particle - Droplet collisions in spray drying. Ph.D. dissertation.School of Engineering.University of Queensland.

Huntington D. H. (2004).The influence of the spray drying process on product properties.Drying technology, 22, 6, 1261-1287.

Iveson S.M., Litster J.D., Hapgood K.P., Ennis B.J. (2001) “Nucleation, growth and breakage phenomena in agitated wet granulation processes: a review” Powder technology, 117, 3-39.

Kota K. and Langrish T. A. G. (2006).Fluxes and patterns of wall deposits for skim milk in a pilot-scale spray dryer. Drying technology, 24, 8, 993-1001.

Kota K., and Langrish T.A.G. (2007).Prediciton of wall deposition behaviour in a pilot-scale spray dryer using deposition correlations for pipe flows. Journal of Zhejiang University Science A, 2007; 8: 301–312.

Kuschel M. and Sommerfeld M. (2013).Investigation of droplet collisions for solutions with different solids content.Experiments in Fluids, 54, 1440.

Langrish T.A. and Zbiciński I. (1994).The effects of air inlet geometry and spray cone angle on the wall deposition rate in spray dryers. Chemical engineering research and design. 72, A3, 420-430

Liao, Y. and Lucas, D. (2010). A literature review on mechanisms and models for the coalescence process of fluid particles. Chemical Engineering Science, 65, 2851–2864

Liu L.X., Iveson S.M., Litster J.D. Ennis. B.J. (2000).Coalescence of deformable granules in wet granulation processes.AIChE, 46, 529-539.

Levelspiel O. (2004). Ingeniería de las reacciones químicas. Limusa Wiley. 3rd Ed, 12, 284 - 285. ISBN 968-18-5860-3.

Marshall J.S. (2007).Particle aggregation and capture by walls in a particulate aerosol channel flow. Journal of aerosol science, 38, 333 – 351.

Ozmen L. and Langrish T.A.G. (2003) An experimental investigation of the wall deposition of milk powder in a pilot-scale spray dryer. Drying technology, 21, 7, 1235–1252.

Palzer S. (2011). Agglomeration of pharmaceutical, detergent, chemical and food powders.Similarities and differences of materials and processes. Powder technology, 206, 2–17

Papavergos P.G. and Hedley, A.B. (1984).Particle deposition behaviour from turbulent flows. Chemical Engineering Research and Design, 62, 5, 275–295.

Podvysotsky A.M. and Shraiber A.A. (1984).Coalescence and break-up of drops in two-phase flows.International journal multiphase flow, 10, 195-209.

Post, S.L., Abraham, J. (2002). Modeling the outcome of drop–drop collisions in Diesel sprays. International Journal of Multiphase Flow, 28, 997–1019

Qian J. and Law C.K. (1997). Regimes of coalescence and separation in droplet collision.Journal of fluid mechanics, 331, 59-80.

Reeks M.W. and Hall D. (2001). Kinetic models for particle resuspension in turbulent flows: theory and measurement. Aerosol science, 32, 1, 31.

Reeks, M.W., Reed, J., Hall ,D. (1988). The resuspension of small particles by a turbulent flow.Journal of physics D, 21, 574-589.

Rüger, M. Hohmann, S. Sommerfeld, M. and Kohnen, G. (2000). Euler/Lagrange calculations of turbulent sprays: the effect of droplet collisions and coalescence. At. Sprays 10, 47–81.

Soldati A. and Marchioli C. (2009). Physics and modeling of turbulent particle deposition and entrainment: Review of a systematic study.International journal of multiphase Flow, 35, 827-839.

Sommerfeld M. (1992). Modeling of particle-wall collisions in confined gas-particle flows.International journal of multiphase flow, 18, 6, 905-926.

Sommerfeld M. and Huber, N. (1999) Experimental analysis and modeling of particle-wall collisions. International journal of multiphase flow, 25, 6-7, 1457-1489

Tardos G.I. and Gupta R. (1996).Forces generated in solidifying liquid bridges between two small particles. Powder Technology, 87, 2, 175-180.

Vatistas N.T. (1992). Effect of adhesion time on particle deposition: re-entrainment and rolling. Industrial engineering and chemistry research, 31, 6, 1554-1559.

Wang H. and Harb J.N. (1997).Modeling of ash deposition in large-scale combustion facilities burning pulverized coal.Progress in energy and combustion science, 23, 267-282.

Woo M.W., Daud W.R.W., Mujumdar A.S., Tasirin S.M., Talib M.Z.M. (2010). Role of rheological characteristics in amorphous food particle-wall collisions in spray drying. Powder technology, 198, 252-257.

Zhang F., Reeks M. W., Kissane M. (2013). Resuspension of small particles from multilayer deposits in turbulent boundary layers.International conference in multiphase flow.Jeju, South Korea.

Zbogar A., Frandsen F., Jensen P.A., Glarborg P. (2009). Shedding of ash deposits.Progress in energy and combustion science, 35, 31-56.

Ziskind G., Fichman M., Gutfinger C. (1995). Resuspension of particulates from surfaces to turbulent flows.Review and analysis.Journal of aerosol science, 26, 4, 613-644.

Zonta F., Marchioli C., Soldati A. (2013). Particle and droplet deposition in turbulent swirled pipe flow.International journal of multiphase flow, 56, 172-183.

Table 1 [**at 2 column** in a 2 column lay out]

Table 1. Design features and operating conditions for the stages defined in section 3.3.

Tower design parameters									
d/D	0.29	H/D	10.58	$^{*}\Omega_i$	5.1 - 5-4	$^{**}U_{p,Sd}$	$< 2-3\ m/s$	$^{**}U_{p,w}$	$< 10\ m/s$
Stage		$P-1$		$CH-1$		$P-2$	$CH-2$		$P-3$
S: Slurry line; W: Water lines, P: Product in the tower belt, E: elutriated fines, EP: full exiting power ***									
$\bar{M}_s/\bar{M}_{s,P-1}$		1.00 ± 0.02		0		1.00 ± 0.03	0		1.01 ± 0.03
$\bar{M}_w/\Delta\bar{M}_{Eq}$		0		0.88		0	0.88		0
$\bar{M}_E$	($\%\ \bar{M}_{EP}$)	2.8		-		n/a	-		n/a
$\bar{T}_P - \bar{T}_S$	(℃)	-3.5 ± 3.6		-		-2.5 ± 3.9	-		-5.3 ± 4.0
Air: A, IN: inlet and EX: exhaust conditions, C: at the cone.									
$\bar{M}_A/\bar{M}_{A,S_2}$		1.00 ± 0.02		0		0.97 ± 0.03	0		0.97 ± 0.02
$\bar{T}_{A,IN}$	(℃)	264.9 ± 2.6		264.4 ± 1.5		264.4 ± 2.7	267.5 ± 4.0		264.4 ± 4.3
$\bar{T}_{A,EX}$	(℃)	88.3 ± 0.5		108.2 ± 8.1		89.6 ± 0.4	107.2 ± 7.6		91.2 ± 1.9
$\bar{T}_{A,C}$	(℃)	195 - 206		191 - 199		195 - 198	176 - 186		194 - 198
rH_{EX}	(%)	15		6		14	7		14

* *The initial swirl intensity, Ω_i, or swirl number, is defined as the ratio of angular momentum of the inlet flow to the angular momentum in the cylinder based on the superficial velocity times the cylinder radius (Francia et al. 2014a).*

** *Particle sedimentation velocity $U_{p,Sd}$ ranges from negative values to up to $2-3\ m/s$ depending on size. Numerical simulations of the spray estimate wall impact velocities $U_{p,w}$ to be $< 10\ m/s$ for sizes $< 400\ \mu m$. Impacts thereafter occur $< 1-2\ m/s$.*

*** *M: mass rate; rH: relative humidity; $\Delta\bar{M}_{Eq}$: equivalent rate of water contained in the slurry.*

Table 2 [**1 column** in a 2 column lay out]

Table 2. A summary of the statistics of the exit age distribution E of the re-entrained material, given in Figures 12.

Class x_{Max}	t_{16}	t_{50}	t_{84}	$\bar{t}$	$X_{s,o}$
µm	$\times 10^2\ s$	$\times 10^2\ s$	$\times 10^2\ s$	$\times 10^2\ s$	$\times 10^2$
< 150	1.6 ± 0.1	5.0 ± 0.3	15.6 ± 2.1	7.9 ± 0.4	30 ± 2
to 212	1.4 ± 0.1	4.5 ± 0.5	13.5 ± 2.7	7.4 ± 0.6	29 ± 2
to 300	1.4 ± 0.1	4.6 ± 0.6	14.6 ± 3.3	7.6 ± 0.7	23 ± 2
to 425	1.5 ± 0.1	4.9 ± 0.7	15.0 ± 3.4	7.8 ± 0.8	19 ± 1
to 600	1.4 ± 0.1	4.7 ± 0.7	15.1 ± 3.2	7.8 ± 0.7	18 ± 1
to 850	1.5 ± 0.1	5.1 ± 0.8	15.2 ± 3.0	8.1 ± 0.8	21 ± 2
to 1180	1.3 ± 0.1	5.0 ± 1.4	16.0 ± 3.4	8.2 ± 1.0	33 ± 3
to 1700	1.3 ± 0.1	5.1 ± 1.6	17.2 ± 3.4	8.4 ± 0.9	46 ± 3
to 2360	1.2 ± 0.1	4.1 ± 1.5	16.2 ± 3.1	8.1 ± 0.9	34 ± 3
to 3350	1.1 ± 0.1	3.1 ± 0.7	14.5 ± 3.5	7.1 ± 1.0	31 ± 3
> 3350	1.4 ± 0.1	4.0 ± 1.6	16.8 ± 2.0	8.7 ± 0.9	27 ± 2
Total	**1.4 ± 0.1**	**4.7 ± 0.3**	**15.1 ± 1.3**	**7.8 ± 0.3**	**20 ± 1**

List of Figures

Figure 1 [**black & white** in print and in web, **1 column** in a 2 column lay out]

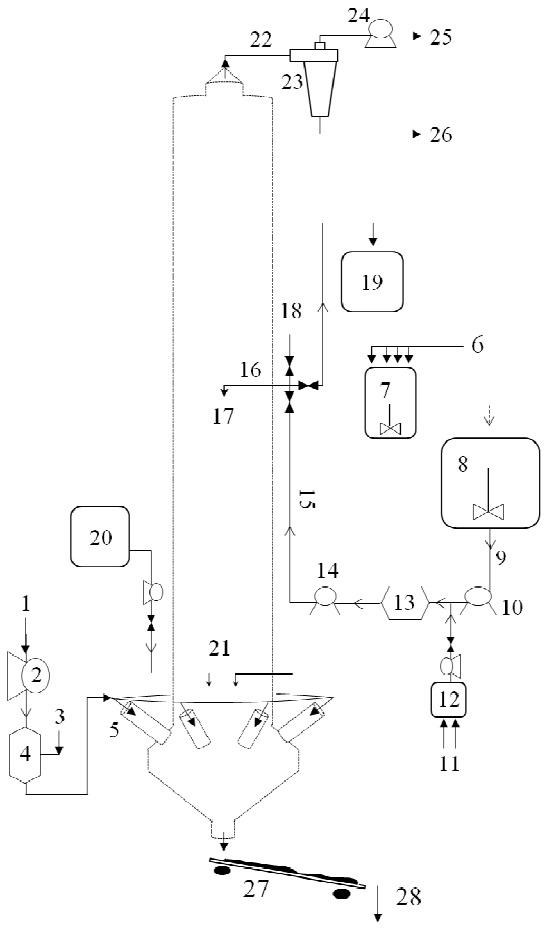

1- Ambient air feed
2- Hot air inlet air fan.
3- Fuel feed.
4- Burner.
5- Hot air inlet nozzle/s.
6- Slurry additions.
7- Crutcher. Batch low shear.
8- Drop tank. Continuous low shear.
9- Low pressure slurry line.
10- Low pressure pump.
11- Tracer and water feeds.
12- Storage. Tarcer aqueous solution.
13- Hammer mill. Continuous high shear.
14- High pressure pump.
16- Nozzle arm.
15- High pressure slurry line.
17- Slurry pressure nozzle.
18- Purge. Air and vapour.
19- Slurry external storage.
20- Storage. Hot water.
21- Water dual nozzle/s.
22- Exhaust air line.
23- Cyclones.
24- Exhaust air fan.
25- Exhaust air oulet.
26- Exit product. Cyclones.
27- Tower belt.
28- Exit product. Tower belt.

Figure 1. A counter-current spray drying system. The configuration of the lines of hot air, slurry and tracer injection.

Figure 2 [black & white in print, **colour** in web, **1 column** in a 2 column lay out]

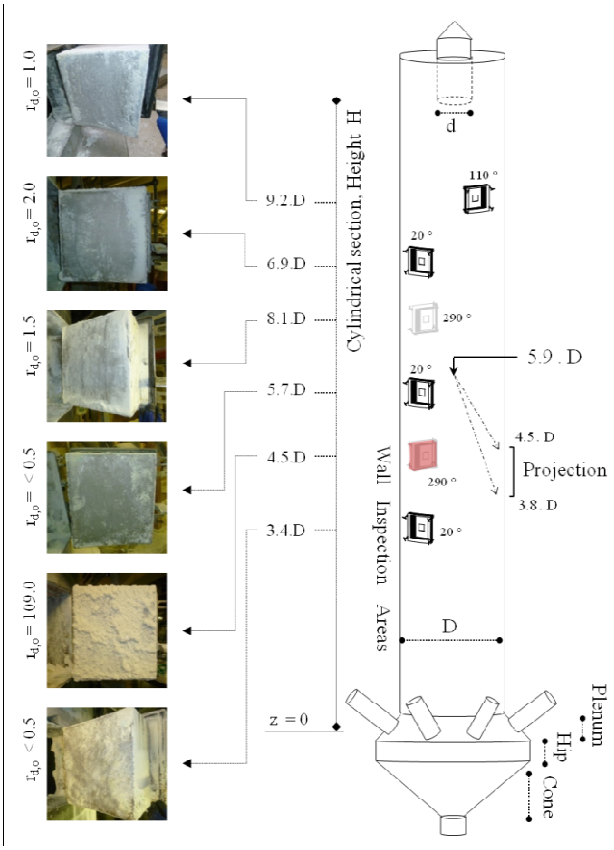

Figure 2. Location of nozzle, wall inspection areas and the projection of the spray cone. Wall deposits axial distribution in a replicate of the experiments described here, initial net deposition rate, $r_{d,o}$ *, given in* $g.min^{-1}.m^{-2}$.

Figure 3 [**black & white** in print and in web, **1 column** in a 2 column lay out]

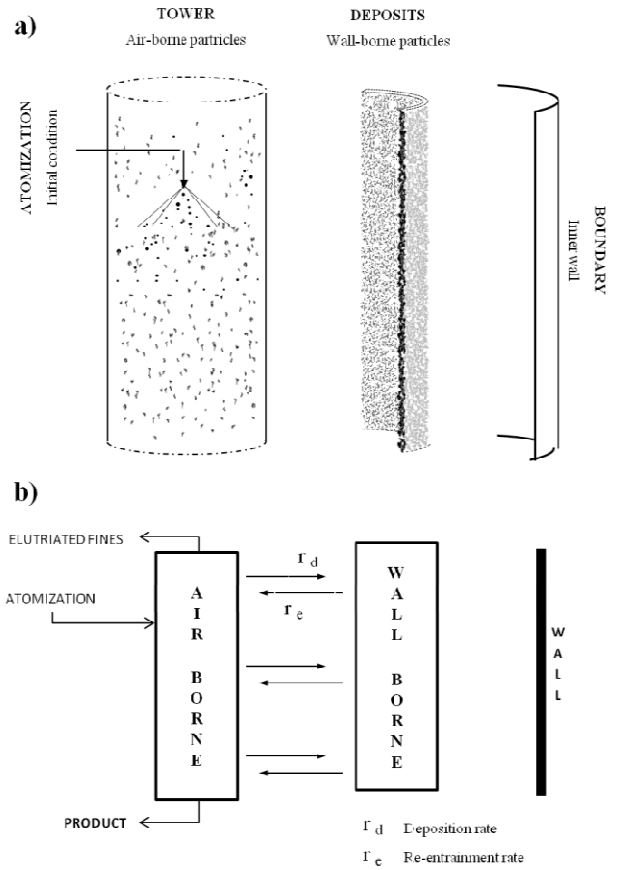

Figure 3. Description of particle history as a combination of two parallel reactors associated to the air and wall borne states.

Figure 4

[**black & white** in print and in web, **1 column** in a 2 column lay out]

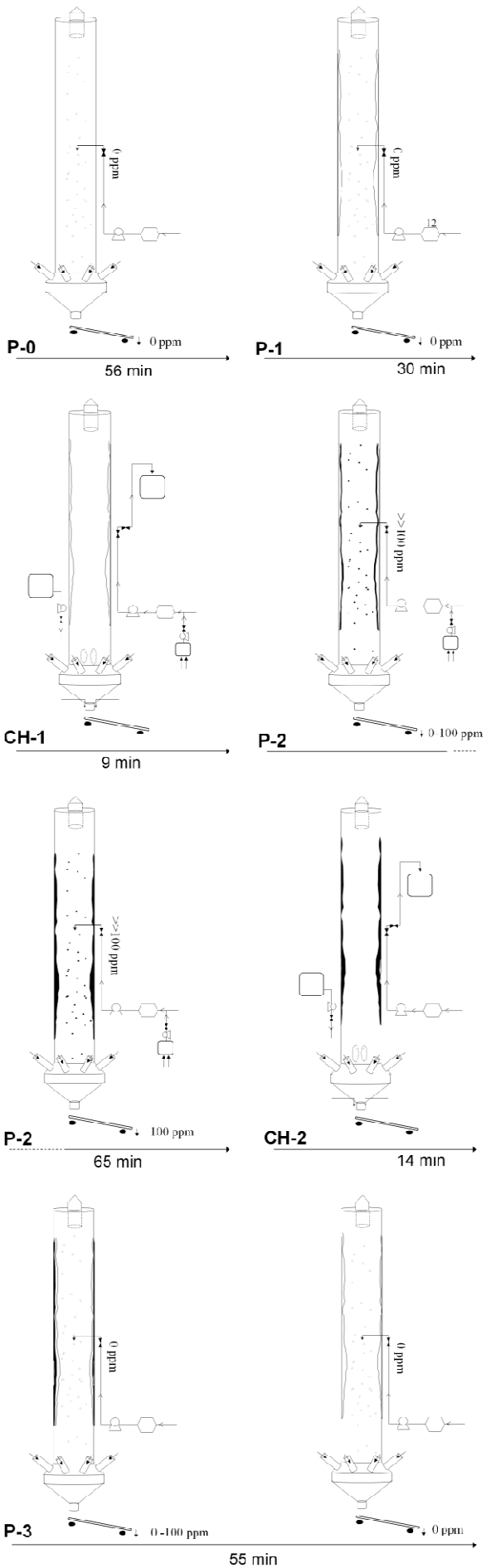

Figure 4. Description of the stages of a tracer experiment sequence.

Figure 5 [**black & white** in print and in web, **1 column** in a 2 column lay out]

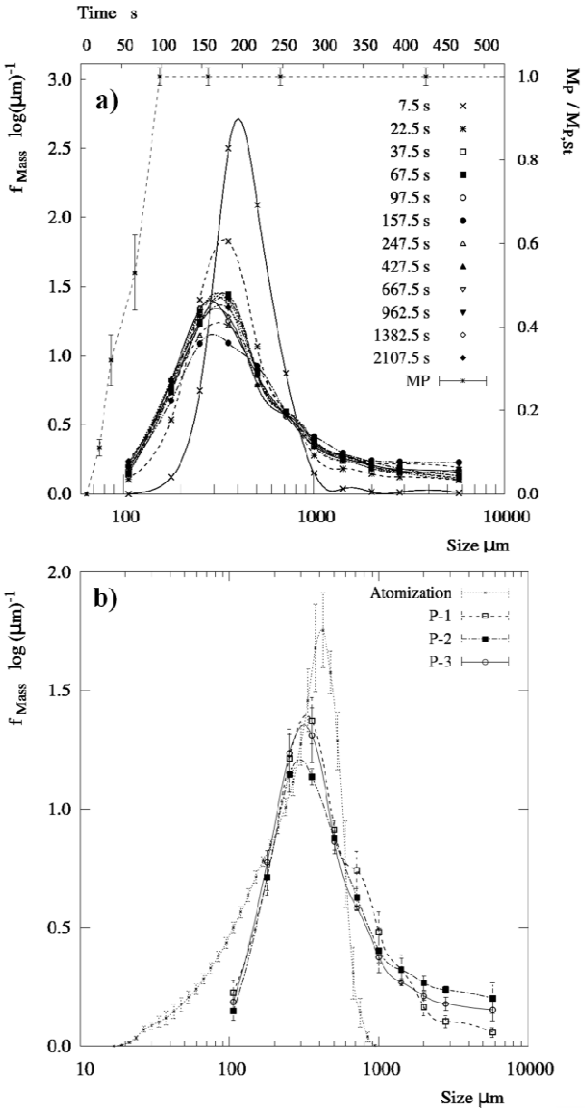

Figure 5. a) Evolution of the tower exit rate and the product weight based size probability density function during the $P-3$. *b) Comparison of the volume based size distribution of the droplets and the product generated during* $P-1$, $P-2$ *and* $P-3$.

Figure 6 [black & white in print, **colour** in web, **1 column** in a 2 column lay out]

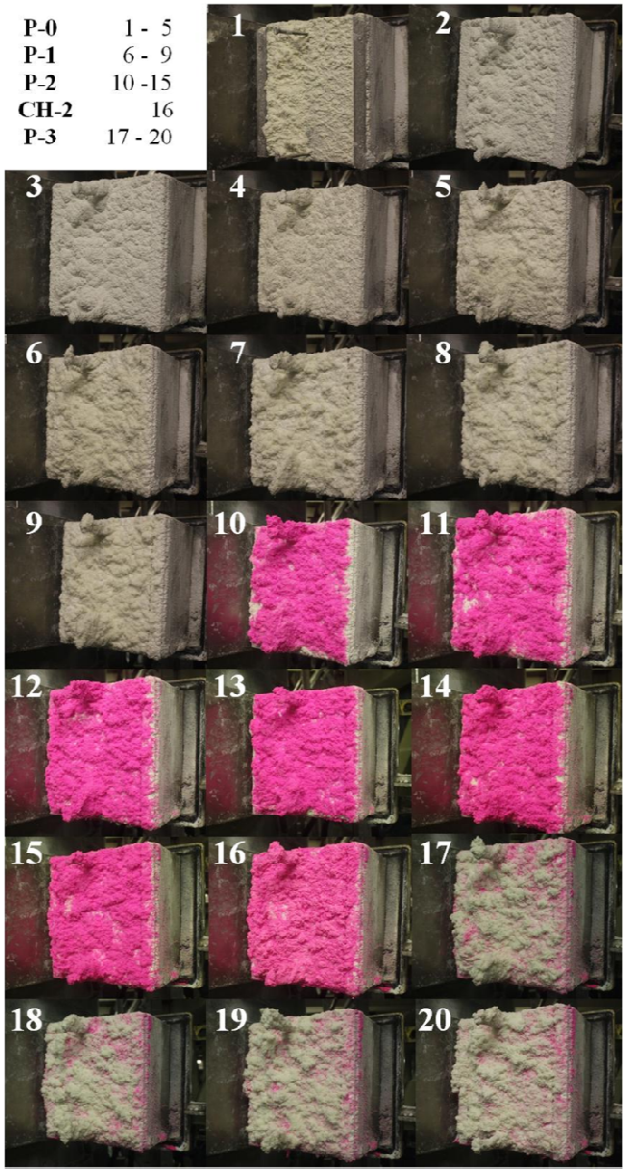

Figure 6. Evolution of the deposits observed at the inspection level 4.5.*D containing the extractable wall plate.*

Figure 7 [**black & white** in print and in web, **1 column** in a 2 column lay out]]

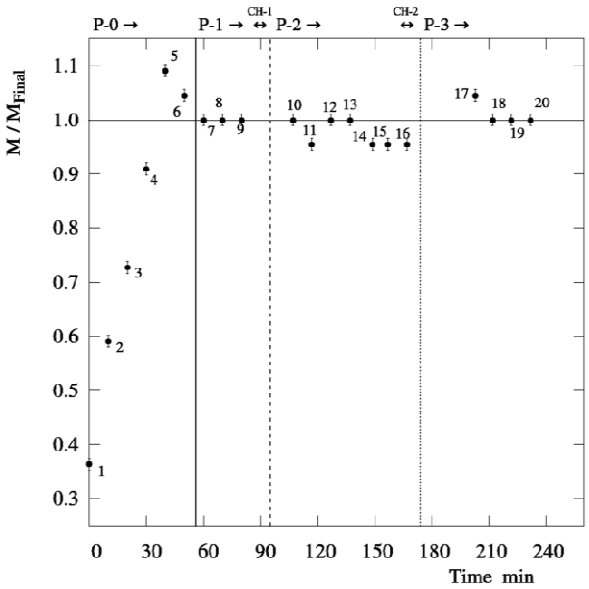

Figure 7. Evolution of the weight of the extractable wall section (plate plus deposit) shown in Figure 6.

Figure 8 [**black & white** in print and in web, **1 column** in a 2 column lay out]

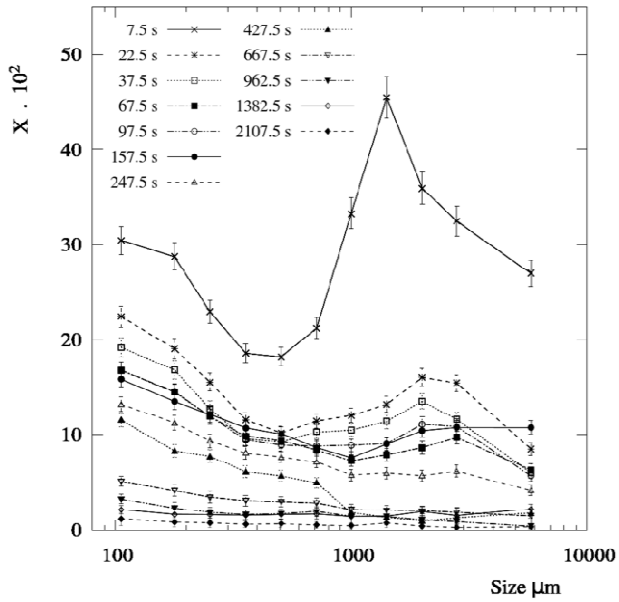

Figure 8. The ratio of material of wall-borne origin, X, in samples taken during $P-3$.

Figure 9 [**black & white** in print and in web, **1 column** in a 2 column lay out]

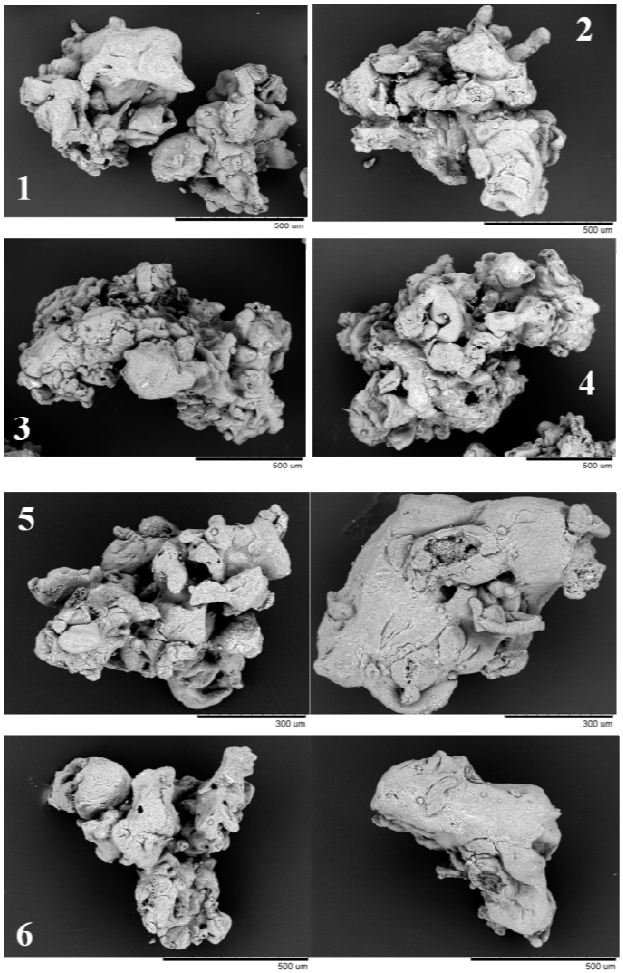

Figure 9. Examples of SEM analysis of large granules. Micrographs (1) correspond to the size fraction $450\ \mu m < x_p < 600\ \mu m$*; (2) to* $600\ \mu m < x_p < 850\ \mu m$*; (3) to* $850 \mu m < x_p < 1180\ \mu m$ *and (4) to* $1180\ \mu m < x_p < 1800\ \mu m$*. Micrographs (5, 2) show both sides of the same granule for the fraction* $450\ \mu m < x_p < 600\ \mu m$.

Figure 10 [black & white in print, **colour** in web, **at 2 column** in a 2 column lay out]

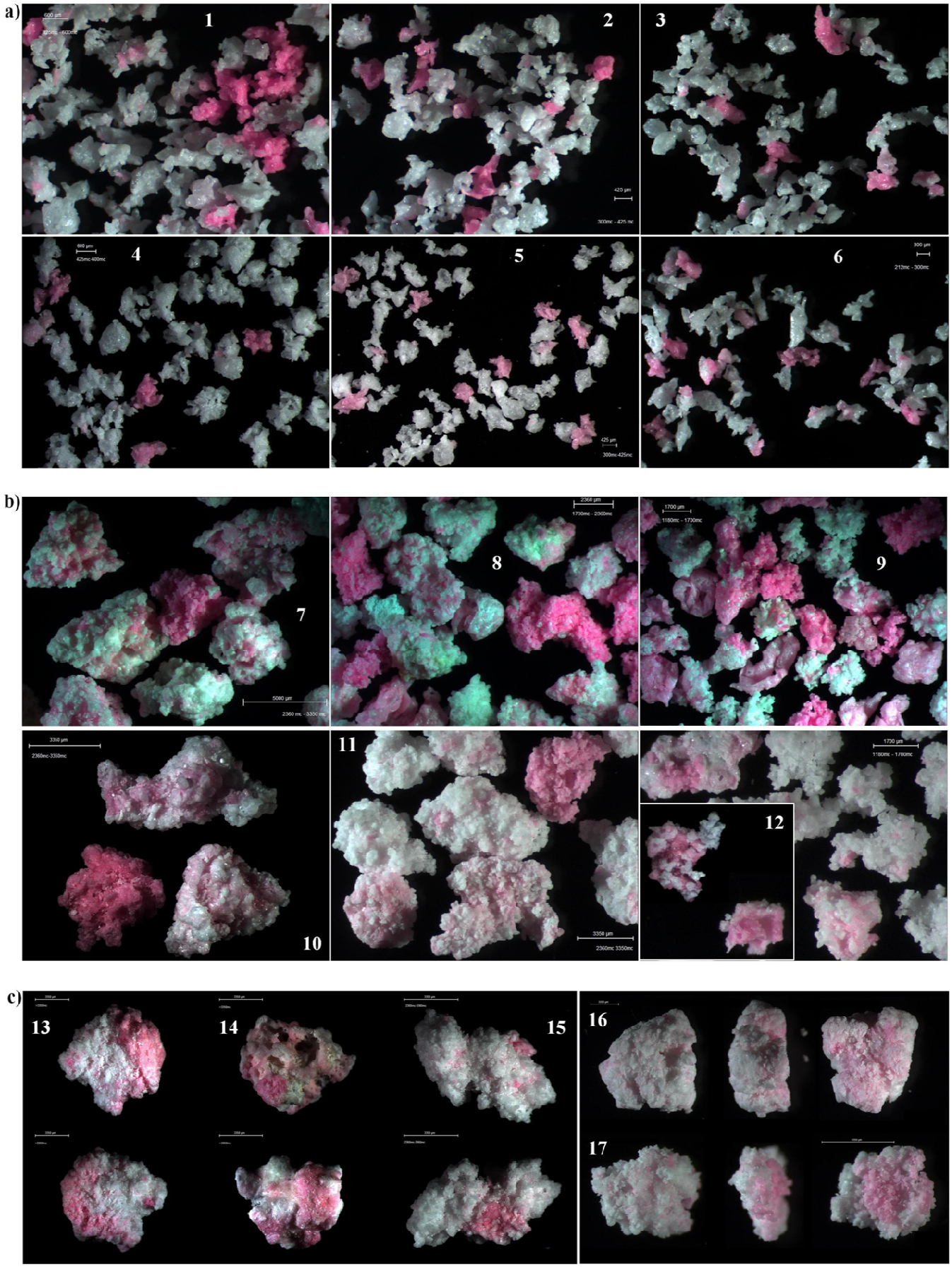

Figure 10. Dye distribution. Examples of optical microscopy. a) pure particles for $x_p < 850\ \mu m$ *b) mixtures for* $x_p > 850\ \mu m$*. c) both sides of large granules (13,14,15) or transversal cuts (16,17). Micrographs of the initial sample* $\sim 7.5\ s$ *are shown in (1 to 3, 7 to 9) and the mode residence time sample* $\sim 157.5\ s$ *in (4 to 6, 10 to 17). Micrographs (1,4) correspond to the fraction* $425\ \mu m < x_p < 600\ \mu m$*; (2,5) to* $300\ \mu m < x_p < 425\ \mu m$*: (3,6) to* $212\ \mu m < x_p < 300\ \mu m$*; (7,10,11) to* $2360\ \mu m < x_p < 3350\ \mu m$*; (8) to* $1700\ \mu m < x_p < 2360\ \mu m$*; (9,10) to* $1180\ \mu m < x_p < 1700\ \mu m$ *and (13 to 17) to* $x_p > 3350\ \mu m$*. See supplementary material for further details.*

Figure 11 [black & white in print, **colour** in web, **1 column** in a 2 column lay out]

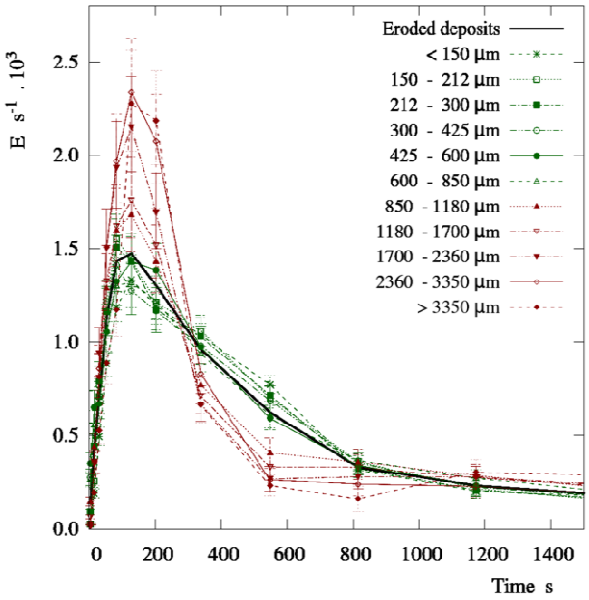

Figure 11. Detail of E. A comparison between the mass averaged values and the functions for all size classes.

Figure 12 [**black & white** in print and in web, **at 2 column** in a 2 column lay out]

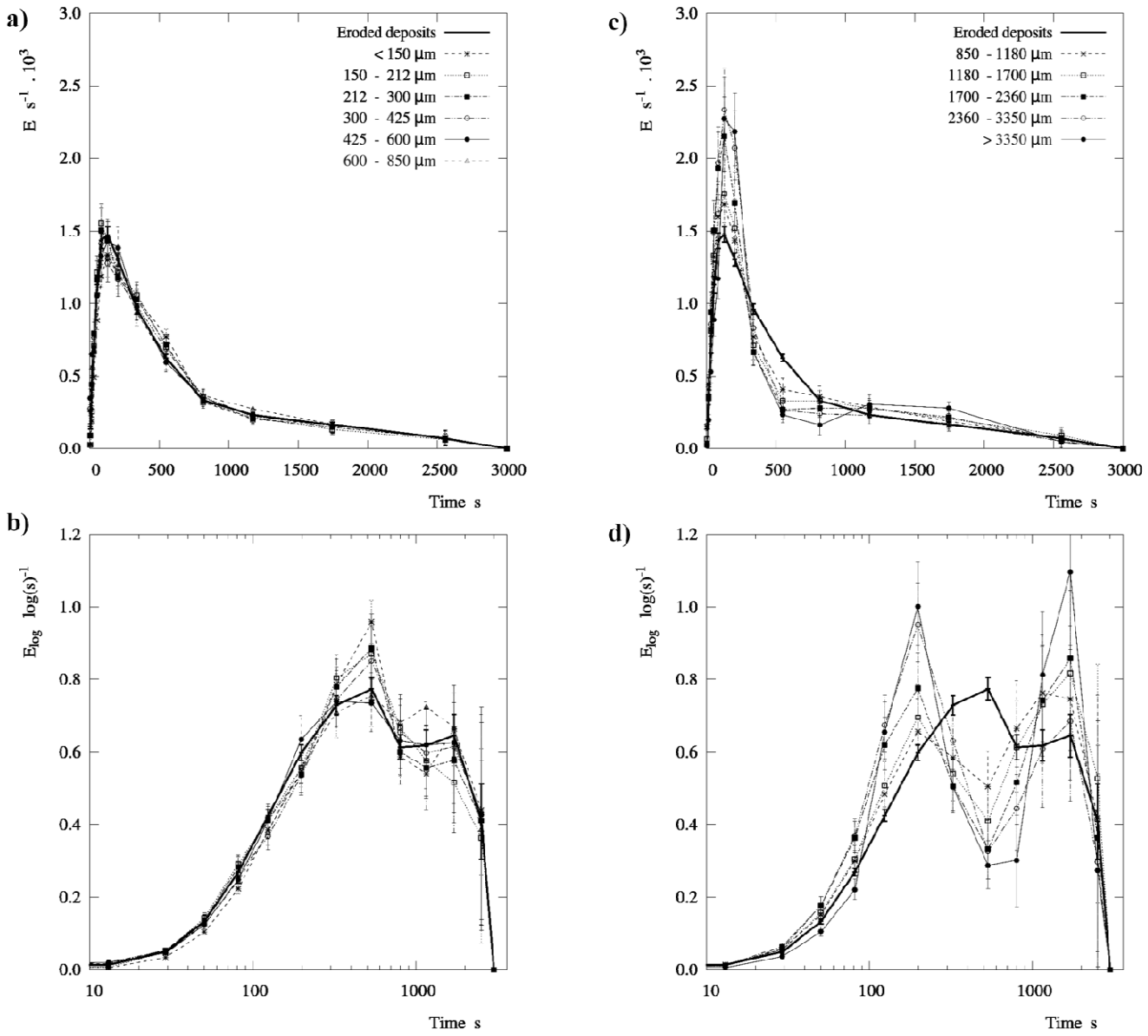

Figure 12. Age distribution of the re-entrained material, E and E_{log}. A comparison between the mass averaged value and the functions for the small and average size classes (a and b) and the large size classes (c and d).

Figure 13 [**black & white** in print and in web, **1 column** in a 2 column lay out]

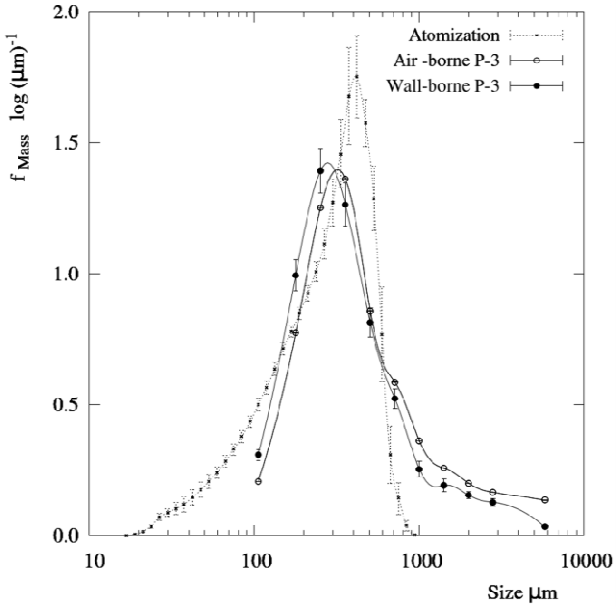

Figure 13. Size probability density functions for the atomization (volume based) and the air and wall borne material (mass based).

Figure 14 [**black & white** in print and in web, **1 column** in a 2 column lay out]

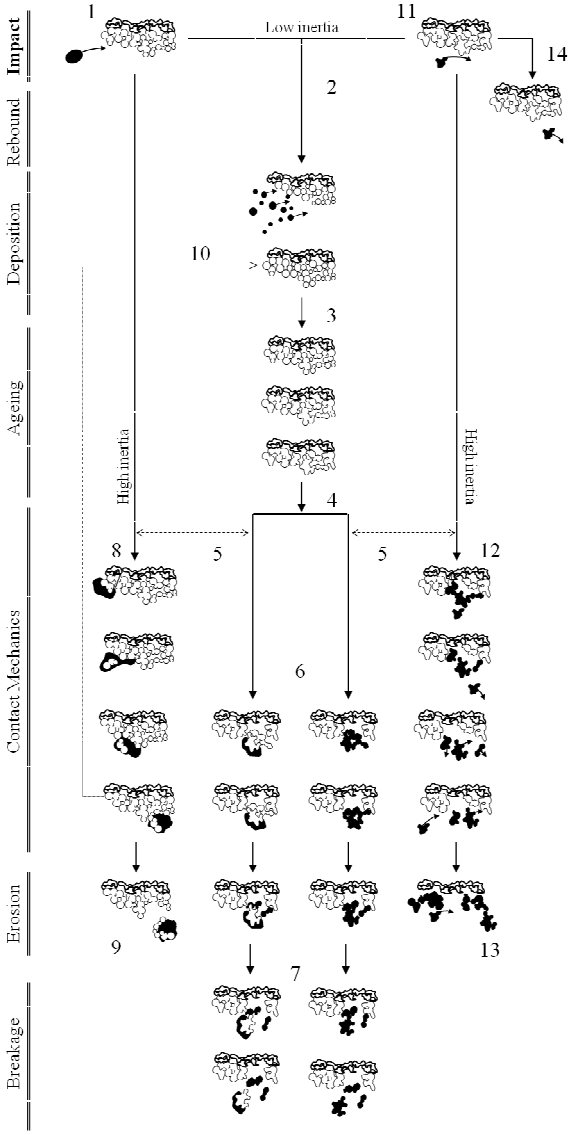

1- Impact of wet / deformable drops
2- Deposition upon impact.
3- Ageing. Sintering / Cristalization.
4- Action of graivty and aerodynamics
5- Trigger by impacts inertia
6- Detachment of large clusters.
7- Break-up of clusters into granules.
8- Encapsulation upon impact.
9- Wet erosion of granules
10- Deposition after capture
11- Impact of dry / rigid particles
12- Breakage of bonds
13- Abrasion of granules.
14- Rebound upon impact.

Figure 14. Wall dynamics in counter-current spray drying. Contact mechanics leading to erosion, aggregation and the breakage of clusters at a multi-layer structure.

Figure 15 [black & white in print, **colour** in web, **1 column** in a 2 column lay out]

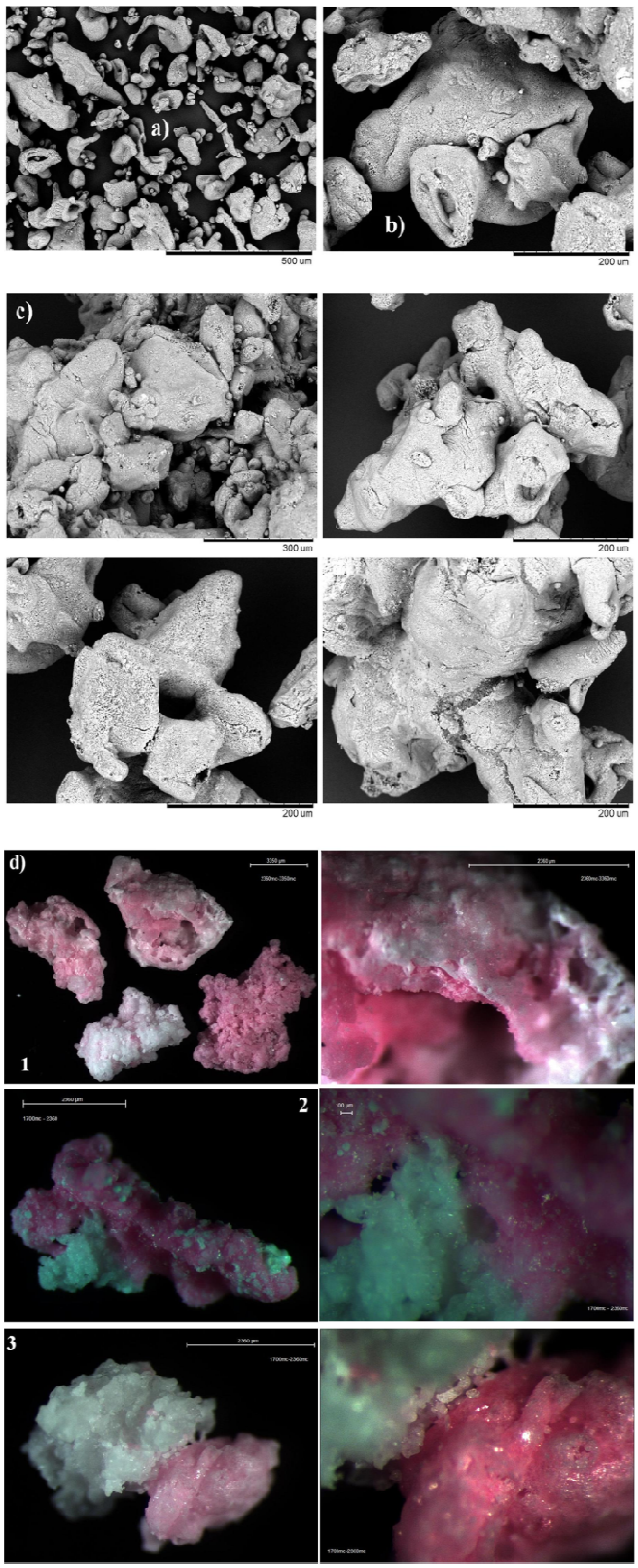

Figure 15. SEM images illustrating a): the presence of ligaments in the elutriated fines b): coiled structures in the product and c), solid bridges and primary particles contacts. d) Optical microscopy illustrating the contacts between the air-borne and wall-borne material, layering in (1), solid bridges of different contact area in (2,3).